

Effects of Thrombosed Vena Cava Filters on Blood Flow: Flow Visualization and Numerical Modeling

SANDY F. C. STEWART, RONALD A. ROBINSON, ROBERT A. NELSON, and RICHARD A. MALINAUSKAS

Office of Science and Engineering Laboratories, Center for Devices and Radiological Health, Food and Drug Administration, White Oak Bldg 62, Rm 2210, 10903 New Hampshire Avenue, Silver Spring, MD 20993, USA

(Received 9 October 2007; accepted 28 August 2008; published online 12 September 2008)

Abstract—Inferior vena cava (IVC) filters are used to prevent pulmonary embolism (PE) in patients with deep vein thrombosis for whom anticoagulation is contraindicated. IVC filters have been shown to be effective in trapping embolized clots and preventing PE; however, among the commercially available designs, the optimal balance of clot capture efficiency, clot dissolution, and prevention of vena cava occlusion is unknown. Clot capture efficiency has been quantified in numerous *in vitro* studies, in which model clots are released into a mock circulation system, with the relative capture efficiency of various IVC filters analyzed statistically. In general, two-stage filters have been found to be more efficient than one-stage filters. However, other factors may play a role in the ultimate dissolution of clots and in the overall effect of the resulting blood flow on caval vasculature. Clot dissolution has been shown to increase with increasing wall shear stress, while low and oscillating wall shear stresses are known to have a deleterious effect on vessel walls, causing intimal hyperplasia. This paper describes the effect of IVC filters on blood flow, velocity patterns, and wall shear stress by flow visualization and computational fluid dynamics.

Keywords—Vena cava filter, Thrombosis, Blood flow, Flow visualization, Computational fluid mechanics, Wall shear stress.

INTRODUCTION

Deep vein thrombosis affects an estimated 48 per 100,000 Americans per year.³⁵ The condition is usually treated by anticoagulant therapy to prevent potentially fatal pulmonary embolism,¹² the incidence of which is estimated at 69 per 100,000 per year,³⁵ with 60,000 dying of the complication per year.¹² In patients for whom anticoagulation is ineffective or contraindicated, a mechanical filter to trap emboli can be placed percutaneously in the inferior vena cava (IVC).¹² The

first IVC filters were designed to mitigate the risks associated with ligation or plication of the vena cava,²⁸ but were subject to obstruction⁸ and migration.²⁹ One design hypothesis is that filters should trap large thromboemboli (which can then undergo lysis by flowing blood), but pass small emboli that can be trapped and lysed in the lungs without serious patient harm.³⁶ Patients with compromised lung function may require a more occlusive filter that traps smaller emboli as well, although with a possibly greater risk of IVC occlusion.^{15,22}

Many IVC filters have been cleared by the U.S. Food and Drug Administration. Today's filters are typically made of flexible stainless steel, titanium, or Nitinol wire. Most use a basic conical shape like the Greenfield⁸ and Vena Tech⁴ filters, which resemble the struts of an umbrella with the opening facing the incoming flow (Fig. 1). Clots are trapped in the center of the filter, with annular flow around the trapped thrombus providing vena cava patency. Other commercial filters vary from this basic design, some with two stages instead of one (e.g., Figs. 1e and 1f).

In Vivo Studies

Good clinical results with the Greenfield filter have been reported, with long-term patency rates of 95%.⁹ In contrast, the two-stage Simon Nitinol filter showed a caval occlusion rate of about 21%.⁷ In a study comparing filters vs. no filters in 400 patients,³¹ the incidence of pulmonary embolism was significantly less in those patients receiving filters. Four filter types were used, but stratification by filter type was not performed. Indeed there has been a dearth of blinded, controlled studies reported in the literature,⁶ thus good clinical data on the *relative* efficacy among filter designs is lacking. The optimal filter design to capture emboli, encourage lysis of trapped thrombus, yet allow good caval blood flow is not yet known.³⁹ The best combination of features is most likely patient

Address correspondence to Sandy F. C. Stewart, Office of Science and Engineering Laboratories, Center for Devices and Radiological Health, Food and Drug Administration, White Oak Bldg 62, Rm 2210, 10903 New Hampshire Avenue, Silver Spring, MD 20993, USA. Electronic mail: sandy.stewart@fda.hhs.gov

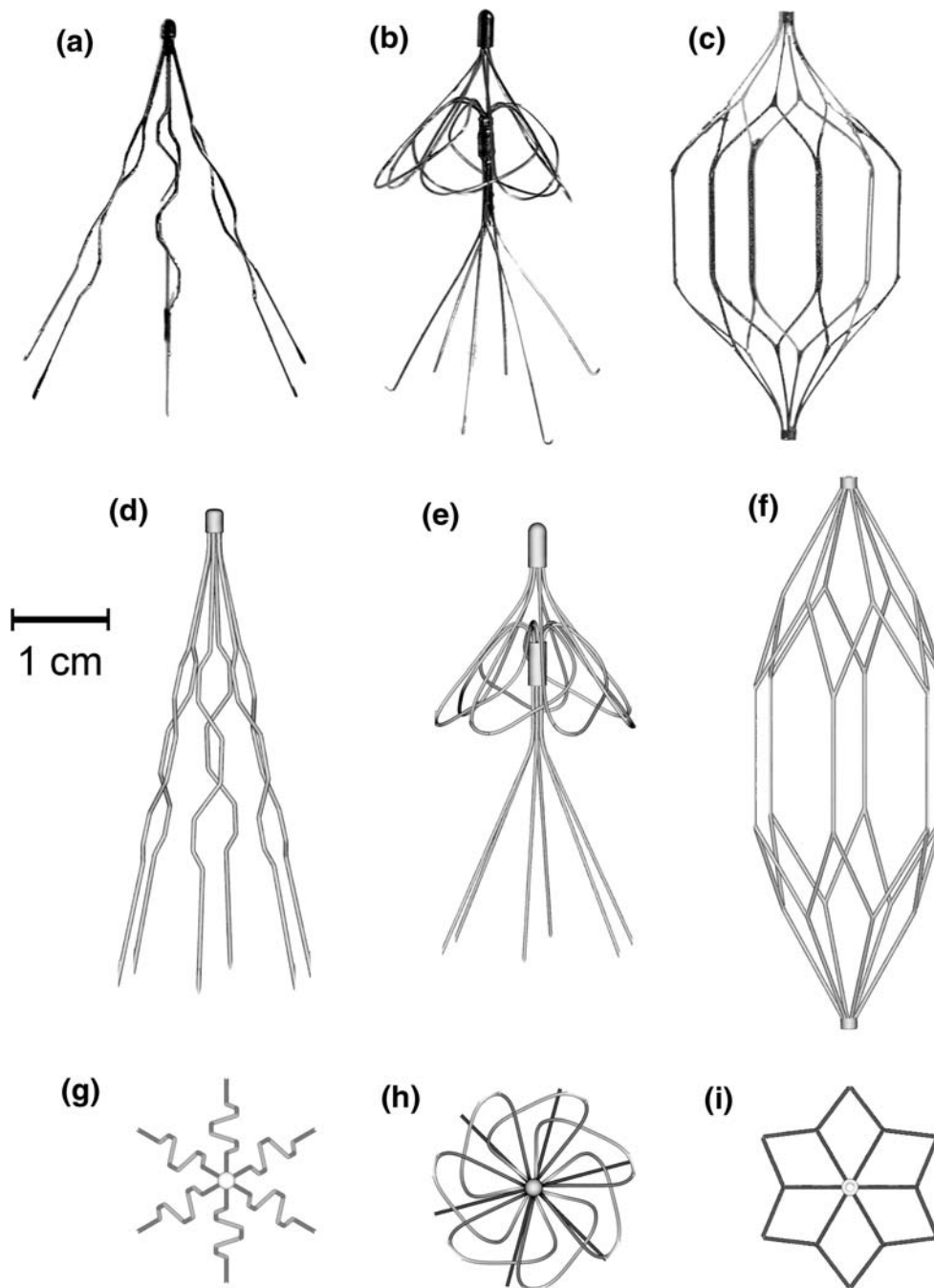


FIGURE 1. Filters used in flow visualizations (shown unconstrained by vena cava): (a) Greenfield; (b) Simon Nitinol; (c) TrapEase. Corresponding computational models (constrained by 2.0 cm inner diameter vena cava): (d) Greenfield; (e) Simon Nitinol; (f) TrapEase. Top views: (g) Greenfield; (h) Simon Nitinol; (i) TrapEase.

dependent, with lung function being an important indicator of the capture efficiency needed.

Some clinical evidence of the clot trapping process has been reported. Radiographs of the two-stage TrapEase filter showed pieces of clot trapped near the wall in the filter's proximal stage, and in the center of the distal stage.³⁰ Caval occlusion in a Vena Tech filter has also been documented by radiography.⁴ A large,

cone-shaped, coiled thrombus was observed to be trapped at the apex of a Vena Tech filter.²⁴ A wall clot (or intimal hyperplasia) was observed in another patient. The Vena Tech filter has an umbrella-strut shape with additional parallel strut wires along the IVC wall. In animal studies of the Vena Tech filter, intimal hyperplasia of the vena cava was observed near the wall struts.¹ Fibrous evolution of trapped thrombus led

to the formation of fibrous webs between the wall struts and IVC wall in a follow-up study.⁵ In a comparison study of stents implanted in the canine aorta and IVC, medial hyperplasia of the IVC associated with thrombus formation led to incorporation of the stent wires into the vessel wall.²⁷

In a comparison of the Greenfield and Vena Tech filters performed in sheep, blood clots 5 mm in diameter by 5, 10, and 30 mm long were injected.²⁶ The Vena Tech filter was found to trap 70 and 100% of the 5 and 10 mm long clots, respectively, while the Greenfield trapped only 26 and 34% of the 5 and 10 mm long clots, respectively. Four out of four Vena Tech filters were occluded with only 2 cm³ of clot, while only two of the four Greenfield filters were occluded, with 4.6 and 8.3 cm³ of clot. This suggests that good trapping efficiency is correlated with a greater tendency for occlusion in these two filters, but whether this rule applies more generally is unknown.

In Vitro Experiments

In an *in vitro* study of nine filters,¹⁵ clot capture efficiency was higher for the Simon Nitinol filter than for the Greenfield filter, with cylindrical clots ≤ 3 mm diameter escaping through the Greenfield but not the Simon Nitinol filter. This is consistent with the clinical results mentioned above. Other *in vitro* studies have confirmed the Simon Nitinol filter to be more efficient at clot capture than the Greenfield filter.^{10,22,37} The two-stage TrapEase filter has also been found to be more efficient than either the Greenfield or Simon Nitinol filter.²²

In vitro flow visualizations have shown that an unobstructed Greenfield filter caused little effect on the flow field.¹¹ A cone-shaped clot occluding the filter caused an annular flow field around the clot. Compared to an empty cylindrical tube, the wall shear stress (WSS) increased seven-fold along the vena cava wall, and tenfold along the clot surface. However, this was not considered to be pathological, leading to hemolysis or thrombogenesis, but in the range to cause clot lysis (as demonstrated in a canine model⁸). No downstream turbulence or flow instabilities were observed.

In contrast, an empty Simon Nitinol filter caused flow stagnation between the distal and proximal stages.¹⁹ The flow was diverted radially to the vena cava wall, thereby doubling the WSS over that in an empty vena cava. A symmetric clot obstructing the filter caused recirculation and stagnation, along with unsteadiness downstream. The maximum WSS on the clot was 30 times that in a simple tube, but decreased to negative values due to the recirculation zone, thus providing a high spatial WSS gradient. Turbulence intensities due to unsteadiness were on the order of 5%.

An unobstructed TrapEase filter showed flow divergence at the proximal tip and lower velocities within the basket.^{20,22} When the TrapEase was obstructed by a symmetric clot in the distal stage, flow diverged around the clot and increased the velocities by 3.6 times. Recirculating and stagnant flow was observed in the clot's wake, extending from the tip of the clot by about 2 cm. Unsteadiness downstream was associated with turbulence intensities reaching 35%. A half-torus clot with elliptical cross-section in the proximal stage next to the wall caused a large zone of stagnant and recirculating flow within the basket downstream of the clot, along the wall of the vena cava. A smaller recirculation zone was present upstream of the clot. No flow instabilities or turbulence were observed.

Thus a major difference among filter designs appears to be the position and symmetry of the trapped clot. The umbrella shape tends to trap thrombi in the center of the filter, allowing annular flow around the clot. However, designs like the TrapEase may also trap thrombi near the wall.²⁰ Caval blood flow is then shunted asymmetrically around the clot. The parallel wires in contact with the IVC wall may also lead to hyperplasia or incorporation into the vessel wall, as has been observed in the Vena Tech filters.^{1,27} The effects *in vivo* of the resulting blood flow asymmetry and WSS on thrombus lysis, aggregation, and intimal hyperplasia is unknown.

The goal of this study was to examine the flow patterns around model clots trapped in three IVC filter designs via flow visualization and computational fluid dynamics (CFD). Clot models were based on radiographic data^{17,24,25} and work by other researchers^{3,11,19,20} presented in the literature. The results were analyzed with respect to recirculation patterns, WSS, and other factors which have been correlated to thrombus lysis or growth, and intimal hyperplasia. This work was intended to help define the relative likelihood and magnitude of risk of hemolysis, thrombosis, and intimal hyperplasia among basic filter designs.

METHODS

In Vitro Experiments

Three commercially available filters were used in the flow visualization studies: a one-stage Greenfield filter (Boston Scientific, Natick, MA, USA), a two-stage Simon Nitinol filter (Bard Peripheral Vascular, Tempe, AZ, USA), and a two-stage TrapEase filter (Cordis, Miami, FL, USA) (Figs. 1a–c). Flow was visualized in a compliant inferior vena cava model made of 0.3 mm thick silicone, nominally 2 cm in inner diameter.

A centrifugal pump was used to drive steady flow at 1.0 L/min, appropriate for the infrarenal vena cava during resting conditions.² The WSS under such conditions was calculated to be 0.74 dyn cm^{-2} . Glycerol (58% by weight) in water at 37°C was used as the blood mimicking fluid, with viscosity ($3.5 \times 10^{-2} \text{ dyn s cm}^{-2}$) and density (1.12 g cm^{-3}) approximating that of whole blood. The fluid used was Newtonian. The model vena cava was suspended horizontally in a bath of blood mimicking fluid, so as to minimize refraction effects. Filters with the wall hooks removed (to prevent rupture of the silicone model) were deployed into the vena cava. The flow system included an asymmetric bifurcation formed by the junction of the iliac veins at the inlet of the inferior vena cava (approximately 15 cm upstream of the filter). The asymmetry was based on human anatomy, with the two branches at 30° and 43° from the vena cava.¹³ The flow loop was typical of those designed for performing clot capture studies.

Models of various size clots were cast of polyvinyl chloride gel (MF Manufacturing, Ft. Worth, TX), with shapes designed to fit into the three filters (Figs. 2 and 3). The clots in the Greenfield and the proximal stage of the Simon Nitinol were based on descriptions and

radiographs of obstructed filters in patients.^{17,24,25} Symmetric cone-shaped clots were fabricated with the downstream angle of the cone configured to match the separation angle of the wires, given the size of the filter deployed in the vena cava (Fig. 2). The clots were made to fill the boundaries of the filter wires; no attempt was made to coil cylindrical clots to fit inside the filters (as might be expected of a long cylindrical clot caught in a filter). Thus it was assumed that real thrombus was sufficiently deformable to pack inside the filters. The upstream ends were hemispherical. Clot diameters were chosen to occlude the filters in a systematically increasing fashion. The cone radii, length, orientation, and angles for the clots used in the Greenfield and Simon Nitinol filters are given in Table 1. Clot sizes were chosen to cover the range that might be expected *in vivo*.

In contrast, 360° ring-shaped model clots as well as 180° symmetric clots were wrapped around the proximal stage of the TrapEase filter (Fig. 3). These clots were based on descriptions and radiographs of clots trapped by the filter published in the literature.^{21,30,33} Table 2 gives the dimensions of these clots. Similar model clots have been used previously in numerous *in vitro* studies.^{3,11,19,20}

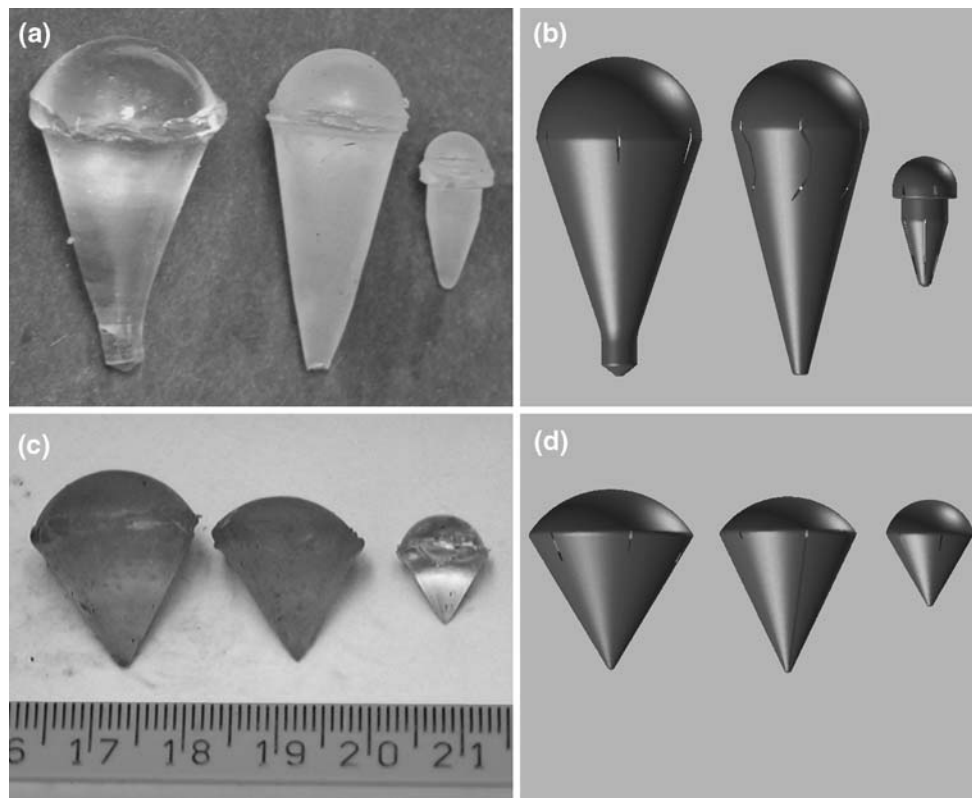


FIGURE 2. Clots used in experimental and computational studies: (a) Greenfield flow visualization clots; (b) Greenfield CFD clots; (c) Simon Nitinol flow visualization clots; (d) Simon Nitinol CFD clots. Visible slots in CFD clots are intersections with filter wires. Scale is in centimeters.

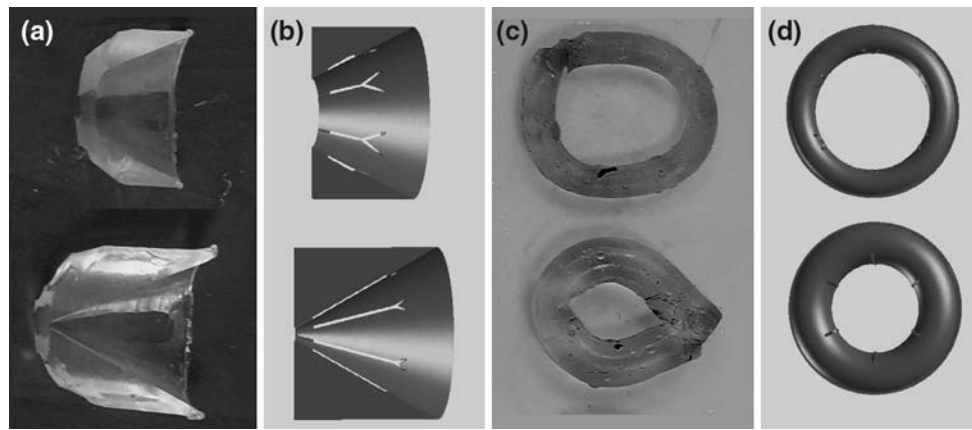


FIGURE 3. Clots used in experimental and computational studies: (a) TrapEase flow visualization 180° asymmetric clots; (b) TrapEase CFD 180° asymmetric clots; (c) TrapEase flow visualization 360° ring clots; (d) TrapEase CFD 360° ring clots.

TABLE 1. Dimensions of clots in Greenfield & Simon Nitinol filters.

Filter	Clot radius (cm)	Clot cone height (cm)	Downstream clot angle (°)	Maximum clot area (cm ²)	Clot volume (cm ³)
Greenfield	0.35	1.28	15.3	0.385	0.25
	0.75	3.00	14.0	1.767	2.65
	0.90	2.70	18.4	2.545	3.82
Simon Nitinol	0.48	0.83	30.0	0.724	0.43
	0.75	1.57	25.5	1.767	1.81
	0.90	1.50	31.0	2.545	2.80

TABLE 2. Dimensions of clots in TrapEase filters.

Filter	Clot	Clot inner radius (cm)	Clot area (cm ²)	Clot volume (cm ³)
TrapEase	Small 180° asymmetric clot	0.40	1.200	0.90
	Large 180° asymmetric clot	0.05	1.700	1.62
	Small 360° ring	0.68	1.689	0.42
	Large 360° ring	0.52	2.292	0.86

Digital Particle Imaging Velocimetry (DPIV) Technique

The blood mimicking fluid was seeded with 20–40 μm polystyrene particles, dyed with a fluorescent dye (Rhodamine 6G and Dichloro-fluorescein dye)¹ that absorbed light at 532 nm and emitted light at 570 nm. The vena cava filter was illuminated by a 532 nm Nd:YAG dual pulsed laser (model Solo I, New Wave Research, Fremont, CA), using a flexible hollow optical fiber.³² A Powell lens (OZ Optics, Ottawa, Canada) was used to spread the laser light emitted from the fiber into a 1 mm thick laser sheet. A

micromanipulator system was used to adjust the laser sheet so that it illuminated the central plane of the filter. A digital CCD camera (model ES 1.0, Kodak, Rochester, NY) was used to record images of the particles illuminated by the laser sheet, with an intervening optical filter used to block the 532 nm light directly from the laser, but pass the 570 nm light emitted by the fluorescent particles. Images were taken at 3–5 positions along the vena cava, from just upstream to just downstream of the filter.

DPIV Analysis

Digital particle imaging velocimetry software (Provision, IDT, Tallahassee, FL) used a cross-correlation algorithm to process pairs of images to provide the velocity fields. A 24×24 pixel interrogation region

¹Obtained from Dr. Yury Ronzhes, Dept. of Mechanical Engineering, The Johns Hopkins University, 223 Latrobe Hall, 3400 North Charles St., Baltimore, MD 21218.

was used. Velocity field data files were then imported into the visualization program, Tecplot (version 10, Tecplot, Inc., Bellevue, WA). Registration of the multiple images per experiment was done manually, by moving the images in the x and y directions until overlapping velocity contours were congruent. Velocity contours and area streamlines were then plotted.

Computational Fluid Dynamics (CFD)

CFD was used in conjunction with the flow visualization studies to provide details on the effects of filters and clots on the flow field. A set of filter/clot/vena cava models were created to match as closely as possible those used in the flow visualizations. Filter dimensional data were obtained by micrometer measurements of the Greenfield, Simon Nitinol, and TrapEase filters used in the flow visualizations. Diagrams in the filters' labeling were also used as a guide. Computer-aided design (CAD) models were then created using the program GAMBIT (version 2.1.6, Ansys, Inc., Evanston, IL) (Figs. 1d–f). The CAD models included the filter wires, the short sections of tubing where the wires come together in the center of the vessel (one tube for the Greenfield, and two each for the Simon Nitinol and TrapEase filter), and the wire struts along the wall (TrapEase only). No attempt was made to model the hooks which imbed in the vessel wall to stabilize the filters. The angles between the filter wires were set so that the filter fit properly within a 2.0 cm inner diameter vena cava. The filters were created with axial symmetry; no attempt was made to model sample to sample variations (e.g., bends, or twists), nor was any attempt made to model a filter tilted within the vessel. Full 360°, three-dimensional models were created. Steady flow simulations were performed in the present study because only steady DPIV data were available.

CFD model clots fitting within the filters were created in GAMBIT to match those used in the flow visualization studies (Figs. 2 and 3, Tables 1 and 2). A 2.0 cm diameter by 24 cm long cylinder was used to model the inferior vena cava, matching the flow visualization studies. No vessel branching or tapering was included, and the vena cava was modeled as having a perfect circular cross-section. The CFD simulated blood clots and vena cava were modeled as being rigid. The iliac veins and bifurcation were not modeled because trial CFD simulations showed that flow from the iliac veins merged together to form a symmetric velocity pattern at the Reynolds numbers used. This may not have been the case in the flow visualizations, due to slight variations in the position of the iliacs, or to differential flow rates in the two branches. To obtain a final CAD model, a filter and clot model were chosen, which were then subtracted from the axial

midpoint of the vena cava model using GAMBIT's solid Boolean functions. In cases where the wires approached the clots or the vessel wall at an oblique angle, small fillets were formed and subtracted from the flow regime to prevent highly skewed elements.

One model per filter type was created with no clot, for comparison. Flow in the vena cava alone (without filter or clot) was also modeled for comparison.

Mesh Design

The final CAD models were meshed using four-node tetragonal elements in the middle third of the vena cava where the filter was situated, and six-node wedge elements in the entrance and exit portions. Hexahedral elements could not be easily used in the filter region due to the complexity of the filter wire topology. The filter wire surfaces were meshed with triangles approximately 0.014 cm on a side, while the clot surfaces were meshed with triangles approximately 0.03 cm on a side. The bulk of the middle third of the vena cava was filled with tetragonals approximately 0.08 cm on a side. GAMBIT's size functions were used to regulate the growth of the elements from small to large. A growth factor of 2 was used in most cases. The models had from 173,270 to 315,719 nodes and from 778,216 to 1,598,601 elements. The mesh for a typical filter/clot/vena cava is shown in Fig. 4 (styled after Swaminathan *et al.*,³⁹ Fig. 2); in this case, the mesh of the Simon Nitinol filter and small clot is shown.

Simulations

Three-dimensional laminar flow in the models was simulated using the program FIDAP (version 8.7.2, Ansys, Inc., Evanston, IL). Three velocity components were simulated: u_z in the axial direction, and u_x and u_y in the plane perpendicular to the axial direction (see Stewart *et al.*,³⁸ Appendix, for discussion of the fluid mechanics equations used). Because of the size of the mesh, FIDAP's segmented solver was used. This solver required a mixed pressure formulation, whereby the pressure variable p was discretized, providing an additional degree of freedom (in contrast to the penalty approach, where the pressure is recovered from the velocities). The clipping parameter for the mixed pressure formulation was set equal to 10^{-8} . The 4-node tetragonal elements used in the meshes required a continuous rather than discontinuous pressure variation over the elements. Positive and negative clipping equal to ± 150 cm/s on the velocity components were also used to suppress oscillations which, in preliminary simulations, led to divergence. Thus if a velocity component at any node increased beyond the clipping threshold during an iteration, the value at that node

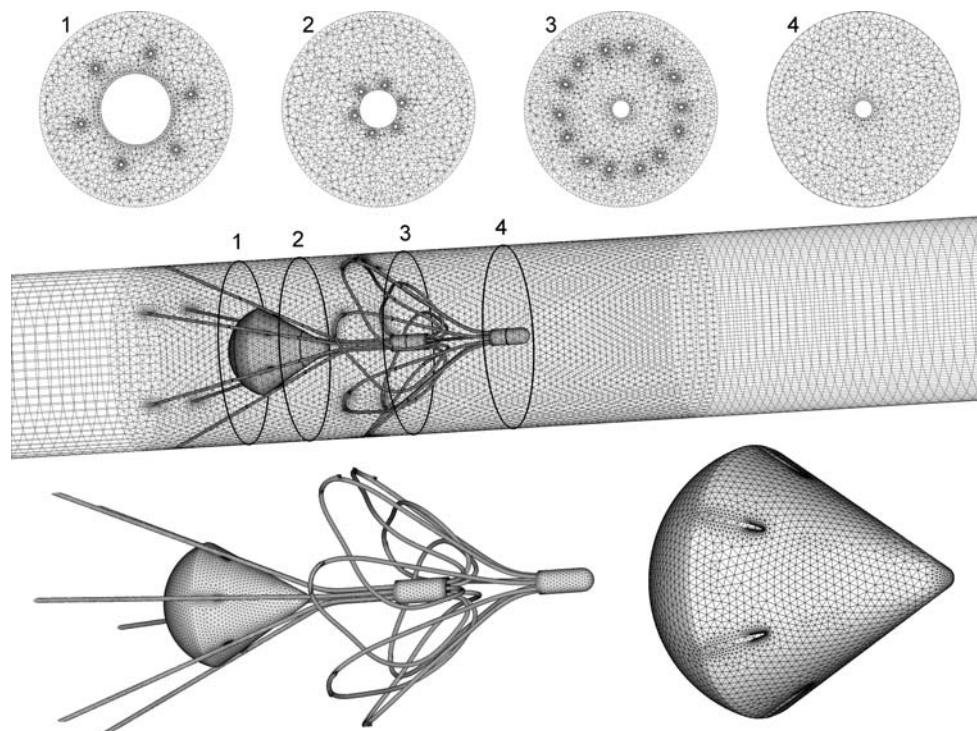


FIGURE 4. Mesh plot of Simon Nitinol filter with small clot. Top: cross-sectional views corresponding to 1, 2, 3, and 4 in overall view. Middle: overall view of vena cava, filter, and small clot. Bottom left: filter with clot in proximal stage. Bottom right: closeup of small clot. After Swaminathan *et al.*,³⁹ Fig. 2.

was reset to the threshold value for the next iteration. The solver used the conjugate residual iterative and conjugate gradient squared methods for solving the symmetric and non-symmetric linear systems of equations, respectively. The convergence tolerance for the two linear systems of equations were both set equal to 10^{-8} , while the overall velocity convergence tolerance was set to 10^{-6} . A simple Newtonian model of blood was used, with the viscosity μ equal to 3.5×10^{-2} dyn s cm⁻² and the density ρ equal to 1.056 g cm⁻³.

A steady parabolic flow profile was applied to the inlet of the vena cava, with velocities calculated to provide a total volume flow rate of 1.0 L/min to match the flow visualization experiments (maximum velocity on the axis = 10.6 cm/s). Natural (stress-free) boundary conditions were automatically applied at the outlet by FIDAP. Zero slip boundary conditions were applied at the wall, filter wires, and clot (if present). The Reynolds number based on the inlet velocity, vessel inner diameter, density, and viscosity ($Re = UD\rho/\mu$) was equal to 320.

A steady, linear simulation was performed first, with zero velocity initial conditions. This solution was then used as input to the final steady, nonlinear simulation. All simulations and analyses were performed on a computer with a 3.0 GHz Pentium 4 processor running Windows 2000.

A mesh refinement study was performed to ensure that the meshes used in the simulations were fine enough to provide accurate results. The vena cava model with the Greenfield filter and medium clot was repeated using 110, 120, and 130% of the original number of nodes. Higher mesh densities were beyond the computer resources available. Computed velocities and shear stresses were then compared at selected coordinates in the four meshes, to determine if the original mesh had sufficiently fine density to not affect the results.

CFD Analysis

The CFD results were analyzed to determine the effects of clot size and configuration on fluid velocities and particle paths, using the program TecPlot 360 (Tecplot, Inc., Bellevue, WA). The velocities and particle paths were compared to the DPIV results. Although the flow patterns around the filters were acknowledged to be three-dimensional, the DPIV technique used was limited to determining the velocities in a two-dimensional plane. Therefore particle paths were calculated in the midplane of the DPIV studies, as well as in the CFD studies for comparison.

The mean wall shear stress, $\bar{\tau}_w$, from the CFD results was also calculated as a function of position on

the filter, clot and vena cava boundaries. The mean shear rate, D , was first calculated by the equation

$$D^2 = 2s_{ij}s_{ij}, \quad (1)$$

where s_{ij} is the strain rate tensor computed using Tecplot's internal functions. Then $\bar{\tau}_w$ was calculated by the equation

$$\bar{\tau}_w = \mu \times D, \quad (2)$$

where μ is the viscosity.

RESULTS

CFD Mesh Refinement Study

Plots of the axial velocity component u_z vs. position (Figs. 5a and 5b) and $\bar{\tau}_w$ vs. position (Fig. 5c) for the four meshes of increasing density showed no substantial quantitative difference among results. Velocity and shear stress data from selected points showed variations of $\pm 5.35\%$ or less (Fig. 5d), and no trends were observed. From these results, we concluded that the original mesh density was fine enough to capture the desired details of flow.

Comparison of Flow Visualizations with Computations

Flow in the empty vena cava showed similar velocity profiles in both the DPIV and CFD results at a point half-way down the 24 cm long vessel (Fig. 6). The CFD results showed the expected parabolic

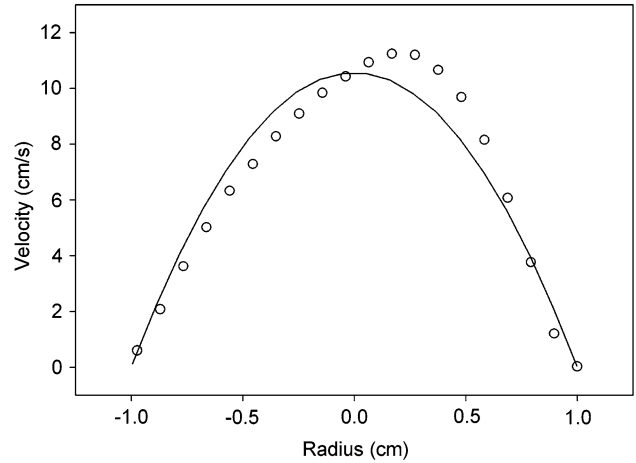


FIGURE 6. Velocity profiles in vena cava with no filter and no clot. Open circles: experiment; solid line: simulation.

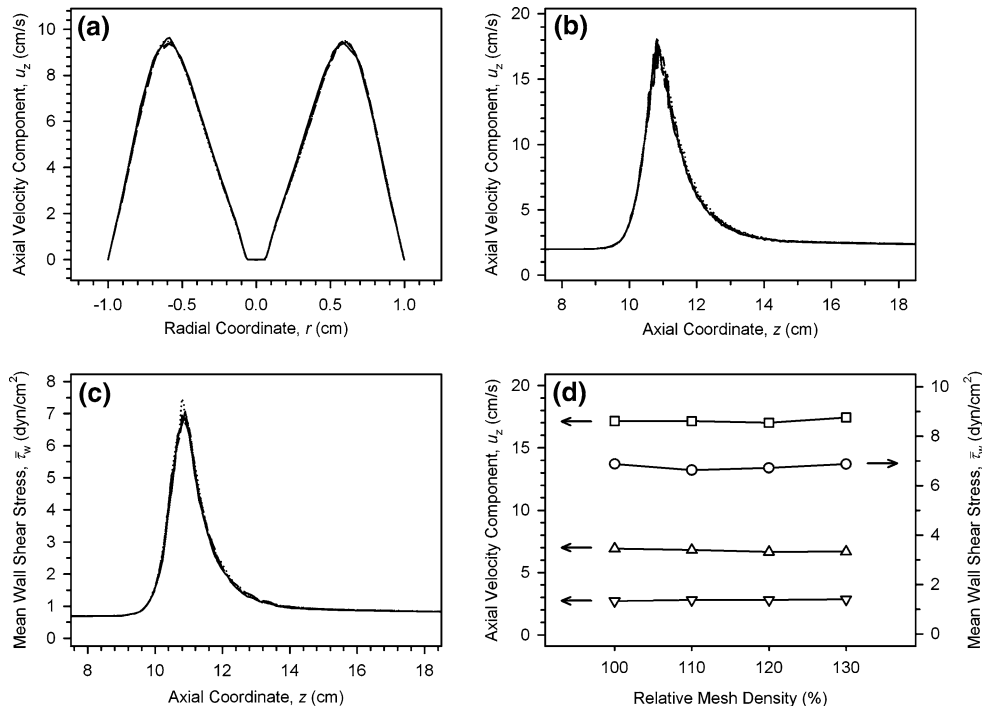


FIGURE 5. CFD mesh refinement study, Greenfield filter with medium clot. (a–c) — original mesh density; — 110% original mesh density; - - - 120% original mesh density; ···· 130% original mesh density. (a) Axial velocity u_z vs. radius r just downstream of clot; (b) axial velocity u_z vs. axial coordinate z at radius = 0.6 cm; (c) mean wall shear stress $\bar{\tau}_w$ vs. axial coordinate z midway between wires; (d) selected data points as a function of mesh density: \square , axial velocity u_z at $(r, \theta, z) = (0.9, 0, -1.13)$ cm (between largest radius of clot and wall); \circ , mean wall shear stress $\bar{\tau}_w$ at $(r, \theta, z) = (0.995, 0, -1.13)$ cm (at largest radius of clot); Δ , axial velocity u_z at $(r, \theta, z) = (0.4, 0, 2)$ cm (just downstream of clot); ∇ , axial velocity u_z at $(r, \theta, z) = (0.9, 0, 2)$ cm (just downstream of clot).

velocity profile, while the flow visualization results showed some non-symmetry. This was likely due to asymmetries in the converging flow from the iliac veins at the input of the physical model, and to the compliance of the vena cava model used, neither of which was simulated in the CFD work. Asymmetries in the converging flow may have also distorted the compliant model somewhat. Despite the lack of symmetry in the experiment, the peak velocities were within 10%: 11.7 cm/s (DPIV) vs. 10.6 cm/s (CFD). The CFD $\bar{\tau}_w$ was equal to 0.73 dyn cm⁻², close to the analytical value of 0.74 dyn cm⁻². The $\bar{\tau}_w$ calculated from the DPIV results were less accurate, equal to 0.40 and 0.50 dyn cm⁻² at the two sides of the wall, respectively, which may be due to the difficulty in the DPIV measurement of velocities close to the wall.

In the vena cava with bare filters, the flow diverged around the wires, then converged on the downstream side. In the empty Greenfield filter (Fig. 7, left panel), the flow was the least diverted due to the simple six wire design, while flow patterns were more complex in both the Simon Nitinol and TrapEase filters (left panels of Figs. 8 and 9, respectively), both of which included a greater number of wire segments. Qualitative agreement between the flow visualization experi-

ments and the CFD results was observed, with differences again due to the asymmetries in the physical models. Velocity profiles were consistent with results from previous studies.^{11,19,20}

In both the Greenfield and Simon Nitinol filters, the trapped clots created more flow interruption and higher flow velocities as the flow diverged radially around the rounded upstream face of the clots, then converged downstream (Figs. 7 and 8, right panels). Flow past the clot in the Simon Nitinol filter caused a small recirculation zone adjacent to the downstream face in both the experiment and simulation (Fig. 8), while no such recirculation zone was observed in the Greenfield filter in either the flow visualization or simulation, presumably due to the smaller, more gradual angle of the Greenfield filter. This is consistent with previously reported results.^{3,11,19}

Flow past the 180° asymmetric clot in the TrapEase filter was qualitatively different, due to the large differences in clot shape and placement (Fig. 9). Flow was diverted to one side by the asymmetric clot, forming recirculation zones both upstream and downstream of the clot visible in both the flow visualization and simulation, as reported previously.²⁰ The size of the downstream recirculation zone was significantly

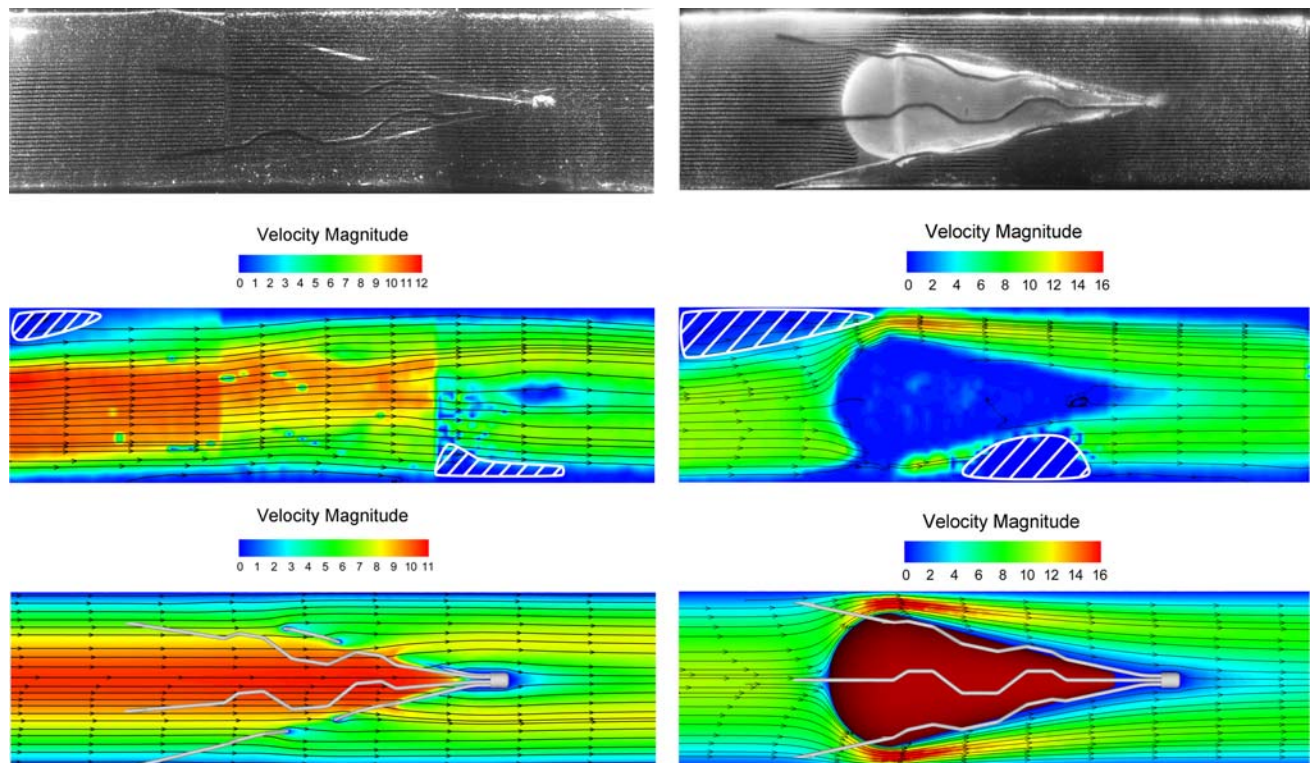


FIGURE 7. Vena cava model (2.0 cm inner diameter) with Greenfield filter, 1.0 L/min flow. Left panels: no clot; right panels, medium clot. Upper panels: DPIV image. Middle panels: velocity magnitude (in cm/s) along central plane from DPIV measurements (white hash marks indicate lighting and shadowing artifacts). Lower panels: velocity magnitude (in cm/s) along central plane from CFD simulation.

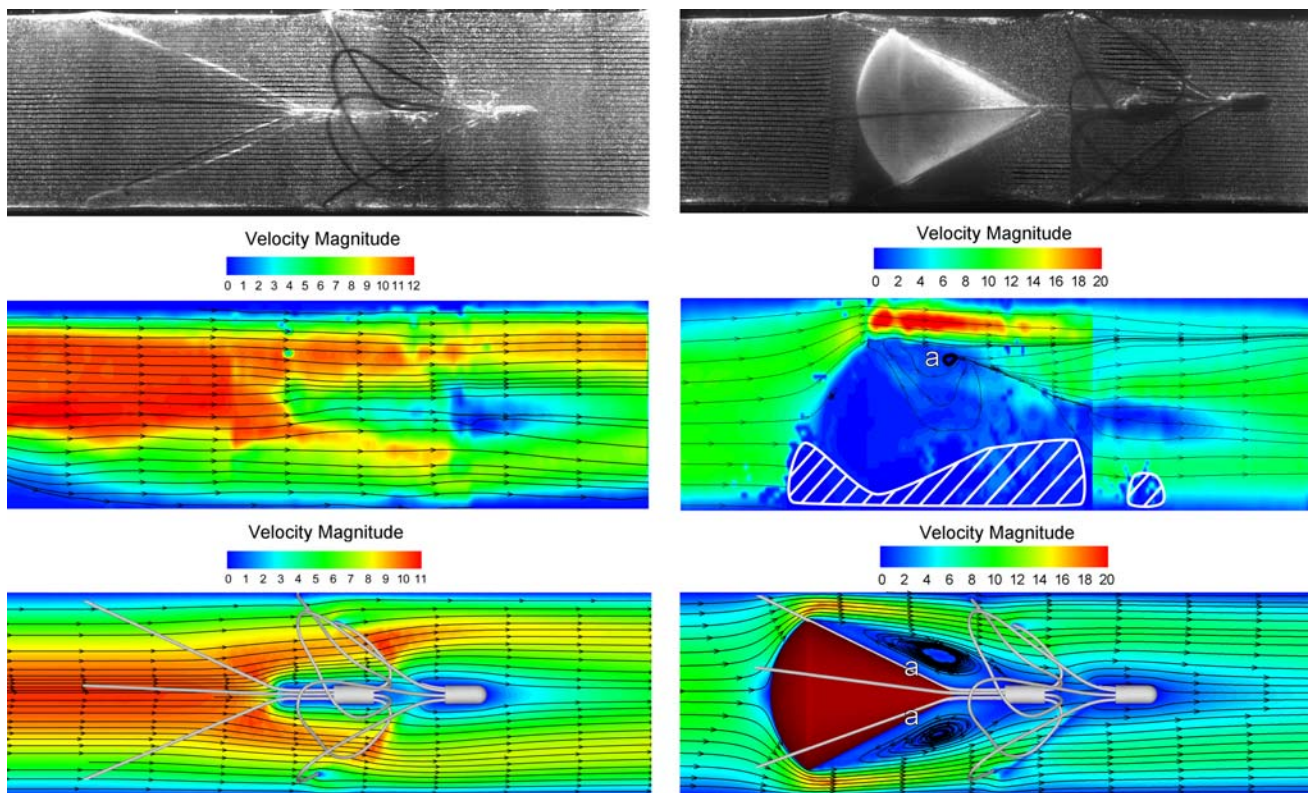


FIGURE 8. Vena cava model (2.0 cm inner diameter) with Simon Nitinol filter, 1.0 L/min flow. Left panels: no clot; right panels, medium clot. Upper panels: DPIV image. Middle panels: velocity magnitude (in cm/s) along central plane from DPIV measurements (white hash marks indicate lighting and shadowing artifacts). Lower panels: velocity magnitude (in cm/s) along central plane from CFD simulation. Points labeled “a” indicate recirculation zones.

different between CFD and DPIV, however. Our CFD results better match those from previous flow visualizations.^{11,20} Flow past the ring clot (Fig. 10) was axisymmetric, forming a high velocity jet in the CFD study that was not visible in the DPIV results, likely due to shadowing of the laser sheet by the filter and clot. Recirculation zones were observed in the DPIV study that were not visible in the CFD study, most likely due to asymmetries present in the former but not the latter. In all cases except the TrapEase/ring clot case, there was good agreement in the maximum velocity observed between the DPIV and CFD studies, which lended support to the validity of the computational results.

Wall Shear Stresses from CFD Studies

In the Greenfield filter, the computed $\bar{\tau}_w$ was lowest ($<0.1 \text{ dyn cm}^{-2}$) around the points of contact with the vena cava (IVC) wall (Fig. 11), compared to a nominal 0.73 dyn cm^{-2} on the IVC wall with no filter. A wavy pattern of IVC $\bar{\tau}_w$ could be seen in the filter with no clot, due to the sinuous design of the filter legs. A centrally located clot caused an increase in $\bar{\tau}_w$ near the maximum

diameter of the clot, similar to that reported previously.³ As the clot size increased, the overall level of $\bar{\tau}_w$ on the IVC wall increased. Similar effects were observed on the Simon Nitinol filter (Fig. 12), although more points of low $\bar{\tau}_w$ were present on the IVC due to the greater number of wires contacting the wall than in the Greenfield filter (13 vs. 6). In the largest clots, streaks of low $\bar{\tau}_w$ could be seen on the IVC wall in the Greenfield filter (Fig. 11d), again as an apparent effect of the wires, while a larger, more complex pattern of low $\bar{\tau}_w$ was observed on the IVC wall in the Simon Nitinol filter (Fig. 12d), due to the curved wires in the distal stage. This latter pattern did not have radial symmetry, because of the mismatch between the proximal six-wire stage and the distal seven-wire stage.

The patterns of $\bar{\tau}_w$ were observed to be more complex in the TrapEase filter. The filter without a clot had larger areas of low $\bar{\tau}_w$ ($<0.1 \text{ dyn cm}^{-2}$) than did the Greenfield (Fig. 13a), due to the six parallel wires in contact with the IVC wall (instead of just the wire ends in the Greenfield filter case). The small 360° ring clot caused a complex radially symmetrical pattern of low $\bar{\tau}_w$ (Fig. 13b), due to recirculation zones downstream of the clot that were broken up by the hexagonal wire

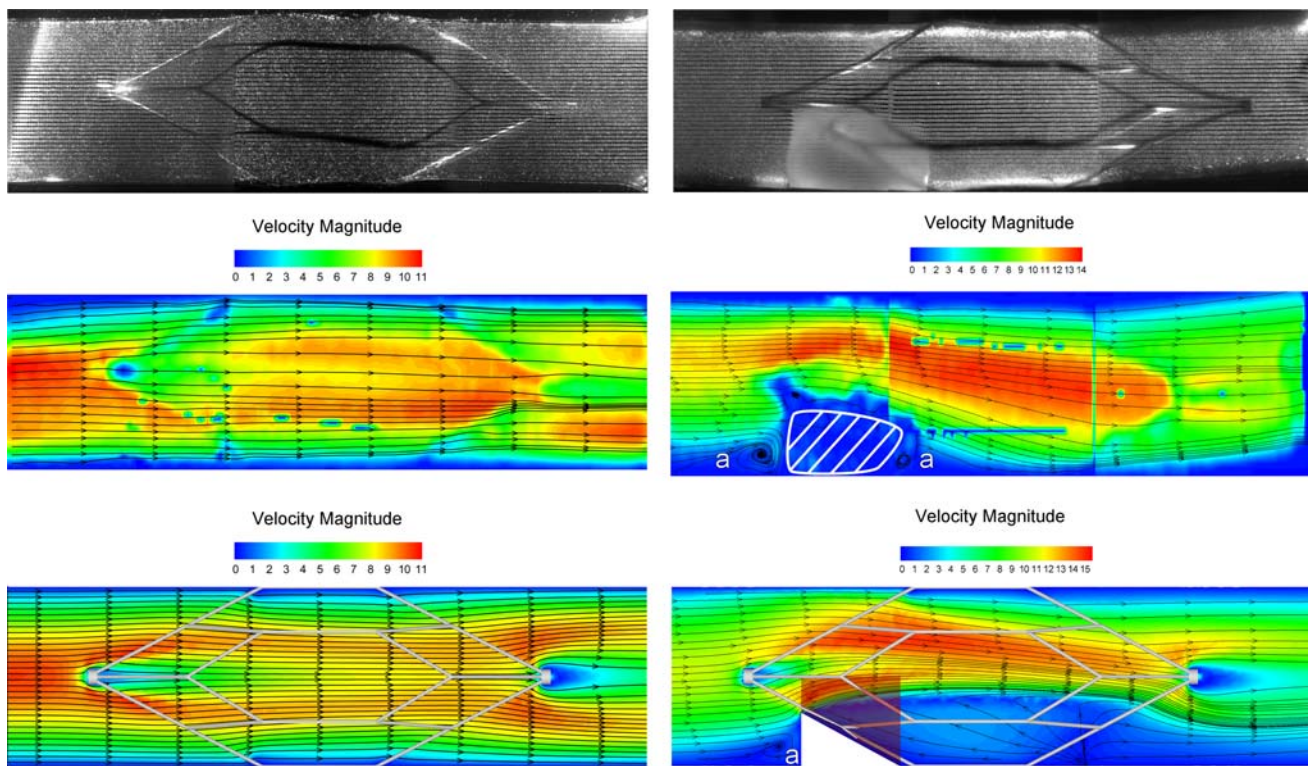


FIGURE 9. Vena cava model (2.0 cm inner diameter) with TrapEase filter, 1.0 L/min flow. Left panels: no clot; right panels, small 180° asymmetric clot (see Fig. 3). Upper panels: DPIV image. Middle panels: velocity magnitude along central plane from DPIV measurements. The white hash marks in this case indicate the position of the clot. Lower panels: velocity magnitude along central plane from CFD simulation. Points labeled “a” indicate recirculation zones.

design. The small 180° asymmetric clot also caused a complex pattern of low $\bar{\tau}_w$ downstream of the clot, that was symmetric about the yz plane (Figs. 13c and 13d). An area of low $\bar{\tau}_w$ upstream of the clot was also observed, due to the recirculation zone upstream of the clot observed in the velocity contour plots (Fig. 9). The $\bar{\tau}_w$ on the clot itself was also seen to be much lower than in the other filters. These trends were also observed in the large 360° ring clot and large 180° asymmetric clot (Fig. 14). Table 3 summarizes the maximum $\bar{\tau}_w$ in all the simulations performed.

DISCUSSION

Patterns of flow past IVC filters without clots were observed to be highly dependent on filter design. Flow past the Greenfield filter was least obstructed, with the flow separating around the wires into six distinct currents that reconnected downstream of the filter. Flow in the Simon Nitinol filter was separated into many more distinct currents, due to the complex pattern of petals in the distal stage, and to the interaction between the six wires of the proximal stage and the seven wires of the distal stage. The downstream flow

was not symmetric as a result of the latter effect. The flow in the TrapEase filter was separated into twelve distinct currents, six in the central portion of the flow and six near the wall. Separation occurred at both the proximal and distal stages of the filter. Flow past the distal stage was affected by the currents formed by the proximal stage.

This distribution of currents influenced the pattern of $\bar{\tau}_w$ on the vena cava wall. The Greenfield filter caused symmetric streaks of low $\bar{\tau}_w$ parallel to the wires. Clots caused bands of higher vena cava $\bar{\tau}_w$, due to fluid speeding up around the obstruction. The magnitude of higher $\bar{\tau}_w$ in the band increased as the clot diameter increased; however, the basic pattern of streaks remained. The Simon Nitinol filter had a different pattern of $\bar{\tau}_w$ due to its two-stage design, and the relative complexity of its flow pattern. Areas of low $\bar{\tau}_w$ were also present around the wires attached to the vena cava wall; however, more such areas were present due to the greater number of wires in contact with the wall in the Simon Nitinol as compared to the Greenfield filter. As with the Greenfield filter, caval $\bar{\tau}_w$ increased with clot size.

The empty TrapEase filter had the largest areas of low vena cava $\bar{\tau}_w$, due to the six parallel wires in direct

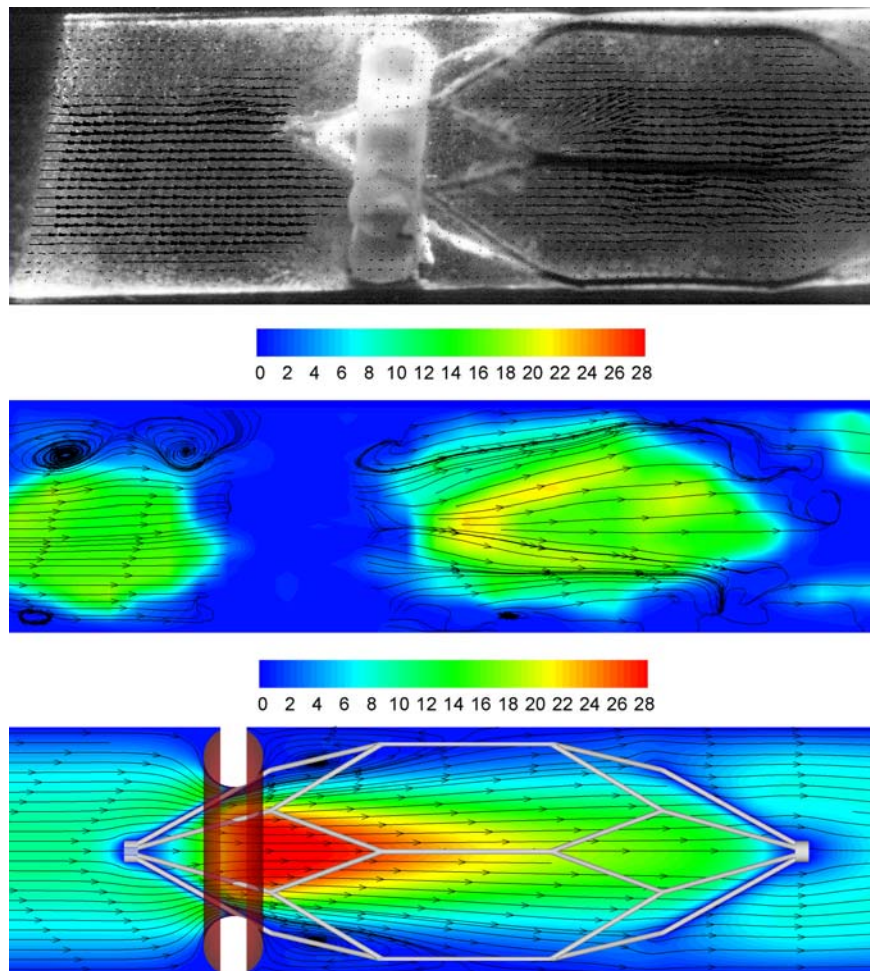


FIGURE 10. Vena cava model (2.0 cm inner diameter) with TrapEase filter and large 360° ring clot, 1.0 L/min flow. Upper panel: DPIV image. Middle panel: velocity magnitude along central plane from DPIV measurements (limited by lighting and shadowing artifacts). Lower panel: velocity magnitude along central plane from CFD simulation.

contact with the caval wall. Furthermore, the 360° ring and 180° asymmetric clots caused large areas of low $\bar{\tau}_w$, due to recirculation zones downstream of the clot (as well as upstream of the asymmetric clots). The clots in the TrapEase filter were much different in shape and size than in the Greenfield or Simon Nitinol filters, but were based on clinical radiographs and clot capture distribution studies. Thus the observed differences may be considered to be fairly representative of the clinical situation. Furthermore, the maximum clot volume in the TrapEase case was 1.62 cm³ (large 180° asymmetric clot, Table 2), compared to 3.82 and 2.80 cm³ in the Greenfield and Simon Nitinol filters, respectively (Table 1); thus smaller clot volumes in the TrapEase cause more complex $\bar{\tau}_w$ patterns. The clinical significance of this is unknown; however, low and oscillating $\bar{\tau}_w$ and high $\bar{\tau}_w$ gradients have been linked to the migration and growth of vascular smooth muscle cells,⁴⁰ and the formation of intimal hyperplasia.¹⁶ Studies have suggested the formation of intimal

hyperplasia near the wall struts of the Vena Tech filter.^{1,24,27} This one-stage filter has parallel wires in contact with the caval wall much like the TrapEase. Low $\bar{\tau}_w$ near the wires may be associated with the formation of hyperplasia observed, but more studies are needed to confirm this.

The $\bar{\tau}_w$ on the downstream ends of the clots was higher in the Simon Nitinol filter than in the Greenfield filter, possibly due to the presence of recirculation zones in the former. This may have an effect on clot dissolution rates, as higher $\bar{\tau}_w$ tends to favor dissolution of the clot,^{18,34} but recirculation and stagnant flow tend to favor aggregation of blood elements and thrombus formation.¹⁴ The relative effects of these two mechanisms in vena cava filters is unknown. However, the differences in flow patterns and $\bar{\tau}_w$ among the three filter designs are consistent with results from previous *in vitro*^{3,11,19,20} and numerical³⁹ studies.

The wall shear stress $\bar{\tau}_w$ can also be compared when similar sized clots are captured by the filters. For

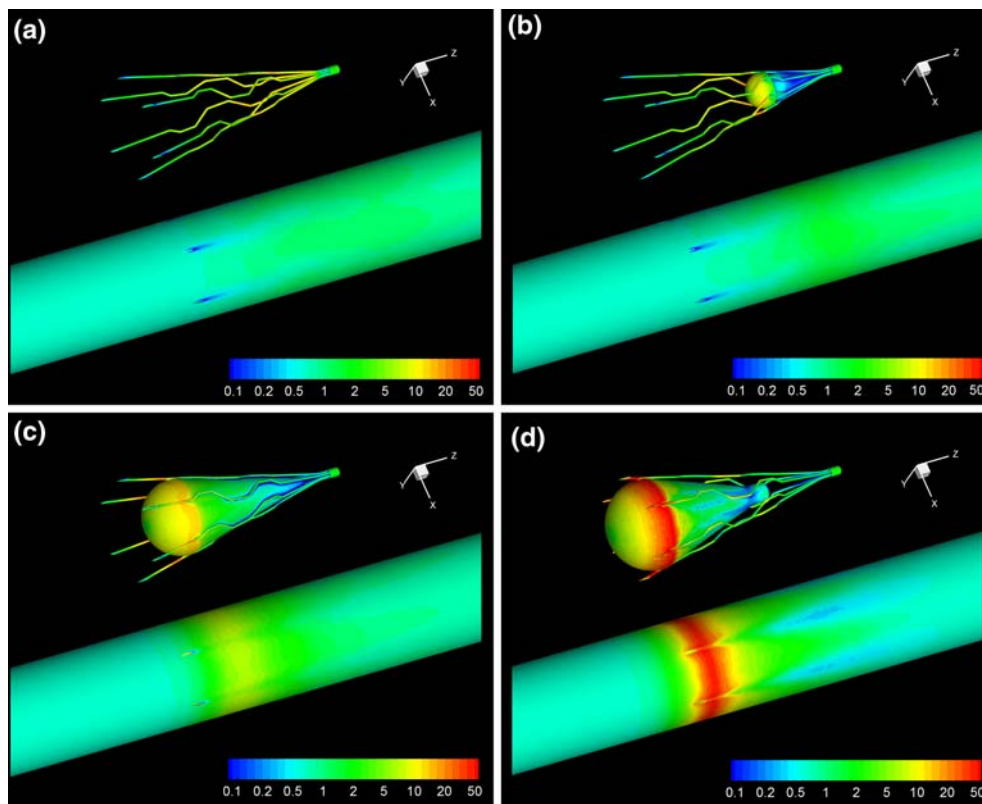


FIGURE 11. $\bar{\tau}_w$ on Greenfield filter and vena cava wall (dyn cm^{-2}) from CFD study. (a) No clot; (b) small clot; (c) medium clot; (d) large clot.

example, from Table 1, the medium clot in the Greenfield filter (volume = 2.65 cm^3) has approximately the same volume as the large clot in the Simon Nitinol filter (2.80 cm^3). From Table 3, we find that the maximum wall shear stress for the Greenfield medium clot is only 28.4 dyn cm^{-2} , compared to 89.3 dyn cm^{-2} ($> 3\times$) for the Simon Nitinol large clot. How the clot volume fills the filters is thus an important difference between the Greenfield and Simon Nitinol filters. However, the proper balance of filtration efficiency, clot dissolution, and potential for caval occlusion remains unknown. Two-stage filters generally have better filtration efficiency than one-stage filters; in a comparative *in vitro* clot capture study of ten filters, the TrapEase and Simon Nitinol were the most efficient in trapping model clots, while the Greenfield filter was the least efficient.²² Similar results have been found in other studies.^{10,15,37} The Greenfield filter may still be useful in patients with healthy lungs that may tolerate small emboli,³⁶ while those with poor pulmonary function may require the greater safety of a more efficient filter, despite the risk of caval occlusion.^{7,15,22}

Regardless of filter efficiency, the position of the captured clot may affect clot dissolution. Theoretically a clot near the wall would be more problematic due to filter occlusion. Based on this study and others,^{11,19}

capturing a clot next to the vena cava wall would seem to be suboptimal. The evidence of recirculation zones and associated low $\bar{\tau}_w$ upstream and downstream of the captured clot do not appear to be conducive to clot dissolution, and may promote continued aggregation of blood elements, clot growth, and intimal hyperplasia. Furthermore, our computational evidence along with recent *in vivo* evidence^{1,24,27} suggests that the total length of filter wires pressing against the vessel wall should be minimized.

Study Limitations

The experimental setup used in this study was designed to provide a realistic test bed for clot capture distribution studies. Flow visualizations were performed to understand behavior of flow around clots; thus a compliant silicone vena cava model was used. The vena cava was supported in a bath of blood mimicking fluid to reduce optical distortion; however, some sagging of the tubes was visible in the DPIV images due to the filter weight. Neither vessel compliance nor curvature was modeled in the CFD simulations. A more accurate CFD model could have been made by characterizing the behavior of the silicone tube and using fluid-structure interaction.³⁸ The tube

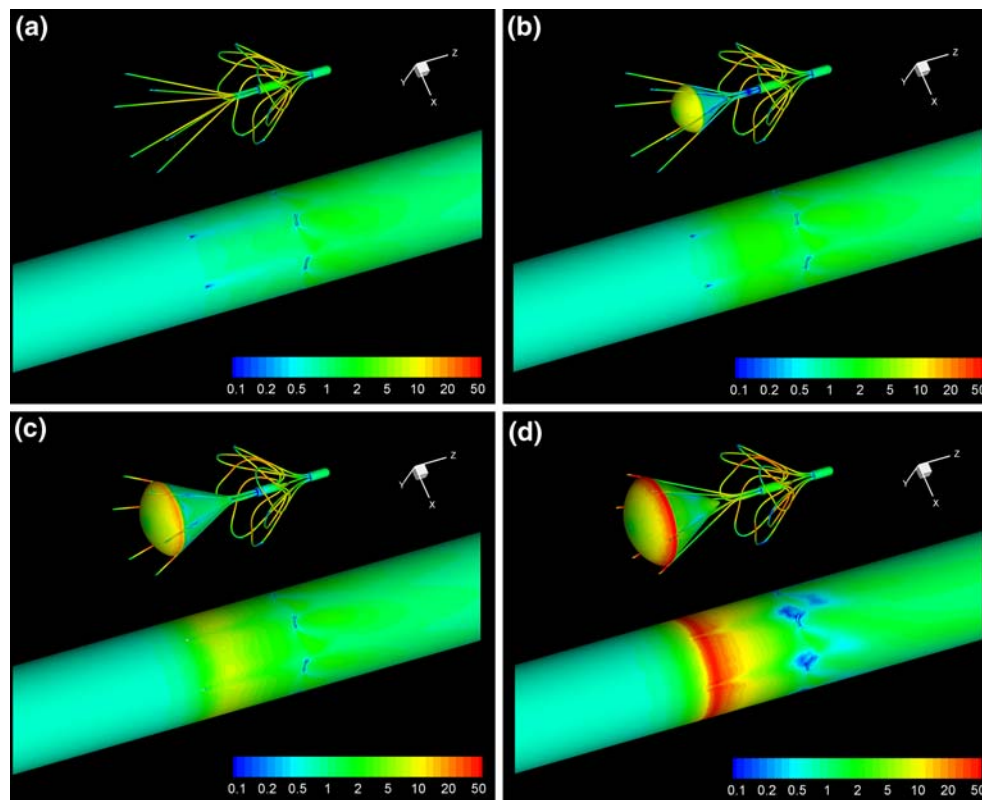


FIGURE 12. $\bar{\tau}_w$ on Simon Nitinol filter and vena cava wall (dyn cm^{-2}) from CFD study. (a) No clot; (b) small clot; (c) medium clot; (d) large clot.

curvature could have been characterized and applied to the CAD model.²³ Both techniques were beyond the scope of this project.

The compliance and slight curvature of the silicone vena cava in the bench experiments also led to difficulty in applying the laser sheet exactly in the centerline of the tube and filters. Some of the differences between the experimental and simulated flow fields may be due to a slight offset of the laser sheet.

The velocities in the DPIV experiment without a filter showed deviations from the expected parabolic profile (Fig. 6). This may have been due to the tube curvature as well as due to the realistic converging iliac veins included in the flow loop, the branches of which may have had slightly different flow rates. The flow rates in the two branches were not measured, so that no data was available as input to the simulations. Therefore a parabolic velocity profile was applied to the vena cava inlet in the CFD studies.

CFD indicated that flow past the filters was fully three dimensional. Slight swirling was seen due to the rotational (but not mirror) symmetry of the Greenfield filter (Fig. 1g), while fully asymmetric flow was seen due to the mismatch between the six-wire proximal stage and seven-wire distal stage in the Simon Nitinol filter (Fig. 1i). Full three-dimensional DPIV studies

were not attempted in the current study, however. Thus the streamlines shown in Figs. 7–10 were constrained to the midplane so that the CFD and DPIV analyses could be compared.

The gel clots used in the DPIV study were difficult to manufacture in smooth shapes. The CAD models were matched to the experimental models so that fine details of the flow patterns could be compared. Other characteristics not captured in the CFD studies (such as tube curvature) prevented the DPIV and CFD flow patterns from matching exactly. These problems could be solved by using a rigid vena cava and clot models. This was not deemed suitable for the clot capture distribution study, however.

This study would have benefited by the use of clots with constant volume from filter to filter. Due to the different configurations of the filters (in particular, the opening angle of the wire baskets), constant volume clots would have different maximum diameters, which would be expected to have different levels of shear stress and maximum velocity. This would provide a better standardized test for direct filter to filter comparisons under equivalent clot loading. We recommend that constant volume clots be considered in the development of national and/or international standard test methods for blood filters of all kinds.

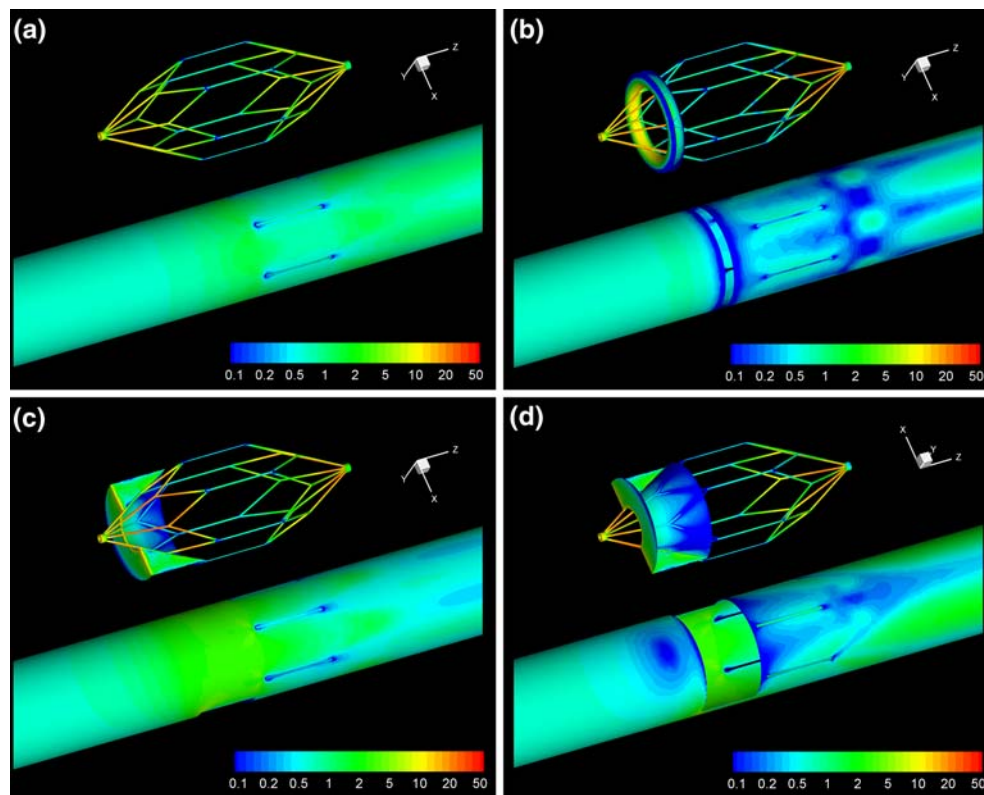


FIGURE 13. $\bar{\tau}_w$ on TrapEase filter and vena cava wall (dyn cm^{-2}) from CFD study. (a) No clot; (b) small 360° ring clot; (c) small 180° asymmetric clot; (d) as in (c), but opposite side of clot.

Shadowing of the laser sheet by the opaque filter and translucent clots occluded significant portions of the flow field. This problem could be addressed by using multiple laser sheets from below and above, or by using a transparent filter model matching the refractive index of the fluid used. Such techniques were outside the scope of our study.

The limitations of the CFD simulation itself included the use of a Newtonian fluid. Blood is known to be non-Newtonian, with a finite yield stress and a viscosity that increases with decreasing shear rate. The effect of the finite yield stress in a recirculation zone downstream of a clot would be to cause a locus of rotating but non-shearing blood in the center of the vortex. Thus a Newtonian solution would lead one to underestimate the residence times of cellular elements, and thus the probability of cellular aggregation. The effect of the nonlinear viscosity would be to decrease the shear rate at low shear stresses just above the yield stress, which would tend to add to this effect. Thus the potential for thrombus growth in a recirculation zone of real blood would probably be greater than what a Newtonian model would suggest.

The complex shapes and angles of the filter wires could not be easily meshed with hexagonal elements, so that less accurate tetragonal elements had to be used.

Minor noise due to the tetragonals can be seen in Fig. 8, lower left panel (jet issuing from the distal stage of Simon Nitinol filter). Noise is also visible in the $\bar{\tau}_w$ plots (e.g., Fig. 11d), amplified due to derivatives being taken. The noise was not expected to significantly affect the results of the study.

A laminar model was used in this study, because the Reynolds number based on the vena cava diameter was 320; however, flow past a blunt object like a clot may have a lower threshold for transition to turbulence. The generation of disturbed flow by vena cava filters has been observed in *in vitro* studies,^{11,19,20} and in a transient numerical study of the Greenfield filter.³⁹ Nonsteady or disturbed flow was not captured in these steady flow simulations, however. Nonsteady or disturbed flows may benefit filters by washing out recirculation zones that otherwise lead to stagnation. Ongoing transient studies in thrombosed filters will be detailed in a future report.

SUMMARY

1. In both *in vitro* and computational studies, substantial differences were observed in the velocity field around three commercially available vena

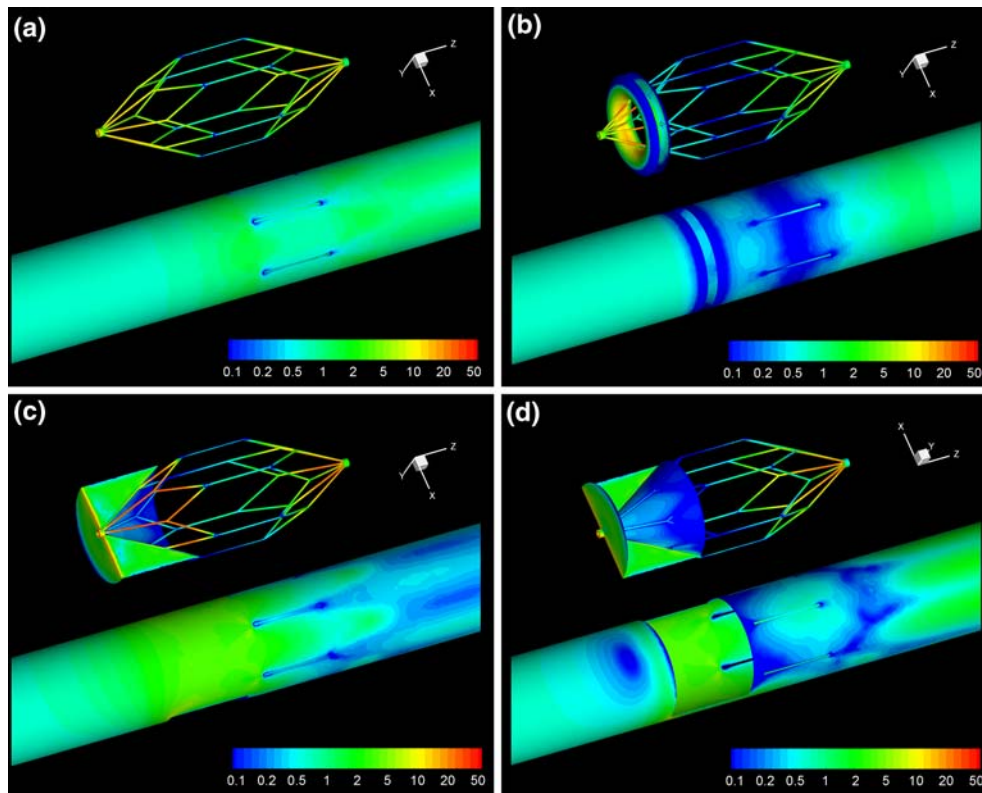


FIGURE 14. $\bar{\tau}_w$ on TrapEase filter and vena cava wall (dyn cm^{-2}) from CFD study. (a) No clot; (b) large 360° ring clot; (c) large 180° asymmetric clot; (d) as in (c), but opposite side of clot.

TABLE 3. Maximum $\bar{\tau}_w$ from computational filter simulations.

Filter	Clot	Maximum $\bar{\tau}_w$ (dyn cm^{-2})			
		Vessel wall	Filter wires	Clot	Overall
Greenfield	None	1.16	18.24	—	18.24
	0.35 cm radius	1.78	23.44	11.23	23.44
	0.75 cm radius	7.96	28.38	16.35	28.38
	0.90 cm radius	54.04	88.41	72.52	88.41
Simon Nitinol	None	2.31	19.64	—	19.64
	0.48 cm radius	2.69	23.68	10.54	23.68
	0.75 cm radius	8.16	36.23	22.27	36.23
	0.90 cm radius	52.93	89.31	74.56	89.31
TrapEase	None	1.67	22.47	—	22.47
	Small 180° asymmetric clot	0.98	25.66	15.34	25.66
	Large 180° asymmetric clot	1.11	28.69	16.37	28.69
	Small 360° ring	7.44	28.03	24.10	28.03
	Large 360° ring	9.56	34.78	24.93	34.78

cava filters. In empty filters, the one-stage Greenfield filter caused less interruption in flow than did the two-stage Simon Nitinol and TrapEase filters, due to its having fewer wires struts.

2. Areas of low shear stress were visible around the points where wires contacted the wall of the vena cava. The relative area of low $\bar{\tau}_w$ due to wire/vessel contact was in the order TrapEase > Simon Nitinol > Greenfield. The consequences of this effect

are unknown, but low $\bar{\tau}_w$ has been linked to intimal hyperplasia. The incorporation of a wall thrombus into the hyperplastic process also may be of concern.

3. Model clots made to fit the natural shape of the filters, based on clot capture studies and radiographs in the literature, further increased the disruption in the flow field. In the Greenfield filter, flow separated around the upstream curved surface,

then rejoined smoothly along the downstream conical surface. In contrast, recirculation zones were seen downstream of the larger clots in the Simon Nitinol filter, most likely due to the larger downstream angle of the clots which encouraged flow separation, and due to the interruption in flow caused by the distal stage. The ring and asymmetric clots in the TrapEase filter also caused recirculating flow due to the blunt downstream configuration. Recirculating flows are known to trap blood elements and encourage thrombogenesis; thus the presence of this flow feature in a vena cava filter would appear to be problematic.

4. Associated with the recirculating flow in the two two-stage filters were areas of low $\bar{\tau}_w$ on the downstream ends of the clots, and on the vena cava wall. Low $\bar{\tau}_w$ may decrease the rate of lysis of blood clots and increase the potential for intimal hyperplasia on the vena cava wall. The relative areas of low $\bar{\tau}_w$ due to the recirculation patterns were in the order TrapEase > Simon Nitinol > Greenfield.
5. Patient characteristics should guide the choice of filter. Patients with good lung function may benefit from single-stage filters, with good trapping efficiency for large emboli, but lower efficiency for smaller emboli which can be safely trapped in healthy lungs. This choice may help prevent the negative effects of blood flow recirculation and thrombogenesis, possible delayed clot lysis due to low $\bar{\tau}_w$, and vena cava occlusion by either clot buildup or intimal hyperplasia. In contrast, patients with poor lung function may benefit from a two-stage filter that has better trapping efficiency even with smaller emboli.
6. Considerations for future two-stage designs include central rather than wall capture of clots, smaller angles of wires (to reduce recirculating flows), and increased distance between stages. This may allow for increased clot capture efficiency without some of the drawbacks of the two-stage filters described herein.

ACKNOWLEDGMENTS

Considerable technical assistance of Dr. Marc Horner of Ansys, Inc., with the finite element simulations is gratefully acknowledged. Discussions with Drs Matthew Myers and William Pritchard of CDRH are also greatly appreciated. We gratefully acknowledge the help of Dr Srilekha Das, who prepared the gel model clots. The mention of commercial products, their source, or their use in connection with material

reported herein is not to be construed as either an actual or implied endorsement of such products by the U.S. Department of Health and Human Services.

REFERENCES

- ¹Bach-Lijour, B., D. Crochet, R. Grossetete, T. Raffin, J. M. Nguyen, M. Hurtrel, G. Daculsi, and J.C. Le Nihouannen. Morphometric study of the wall of the caudal vena cava after the implantation of a filter in the sheep. *Anat. Histol. Embryol.* 27:231–235, 1998. doi:10.1111/j.1439-0264.1998.tb00186.x.
- ²Cheng, C. P., R. J. Herfkens, and C. A. Taylor. Inferior vena caval hemodynamics quantified *in vivo* at rest and during cycling exercise using magnetic resonance imaging. *Am. J. Physiol. Heart Circ. Physiol.* 284:H1161–H1167, 2003.
- ³Couch, G. G., H. Kim, and M. Ojha. *In vitro* assessment of the hemodynamic effects of a partial occlusion in a vena cava filter. *J. Vasc. Surg.* 25:663–672, 1997. doi:10.1016/S0741-5214(97)70293-3.
- ⁴Crochet, D. P., P. Brunel, S. Trogrlic, R. Grossetete, J. L. Auget, and C. Dary. Long-term follow-up of Vena Tech-LGM filter: predictors and frequency of caval occlusion. *J. Vasc. Interv. Radiol.* 10:137–142, 1999. doi:10.1016/S1051-0443(99)70455-0.
- ⁵Crochet, D., R. Grossetete, B. Bach-Lijour, L. Larguier, and J. C. Le Nihouannen. Evaluation of the LGM Vena-Tech infrarenal vena cava filter in an ovine venous thromboembolism model. *J. Vasc. Interv. Radiol.* 12:739–745, 2001. doi:10.1016/S1051-0443(07)61446-8.
- ⁶Girard, P., J. B. Stern, and F. Parent. Medical literature and vena cava filters: so far so weak. *Chest* 122:963–967, 2002.
- ⁷Grassi, C. J., A. H. Matsumoto, and G. P. Teitelbaum. Vena caval occlusion after Simon nitinol filter placement: identification with MR imaging in patients with malignancy. *J. Vasc. Interv. Radiol.* 3:535–539, 1992.
- ⁸Greenfield, L. J., J. R. McCurdy, P. P. Brown, and R. C. Elkins. A new intracaval filter permitting continued flow and resolution of emboli. *Surgery* 73:599–606, 1973.
- ⁹Greenfield, L. J., R. Peyton, S. Crute, and R. Barnes. Greenfield vena caval filter experience: late results in 156 patients. *Arch. Surg.* 116:1451–1456, 1981.
- ¹⁰Hammer, F. D., H. P. Rousseau, F. G. Joffre, B. P. Sentenac, T. Tran-Van, and R. P. Barthelemy. *In vitro* evaluation of vena cava filters. *J. Vasc. Interv. Radiol.* 5:869–876, 1994.
- ¹¹Harlal, A., M. Ojha, and K. W. Johnston. Vena cava filter performance based on hemodynamics and reported thrombosis and pulmonary embolism patterns. *J. Vasc. Interv. Radiol.* 18:103–115, 2007. doi:10.1016/j.jvir.2006.10.020.
- ¹²Hirsh, J., and J. Hoak. Management of deep vein thrombosis and pulmonary embolism. A statement for healthcare professionals from the Council on Thrombosis (in consultation with the Council on Cardiovascular Radiology), American Heart Association. *Circulation* 93:2212–2245, 1996.
- ¹³Jaeger, H. J., T. Mair, M. Geller, R. K. Kinne, A. Christmann, and K. D. Mathias. A physiologic *in vitro*

- model of the inferior vena cava with a computer-controlled flow system for testing of inferior vena cava filters. *Invest. Radiol.* 32:511–522, 1997. doi:[10.1097/00004424-199709000-00003](https://doi.org/10.1097/00004424-199709000-00003).
- ¹⁴Karino, T., and H. L. Goldsmith. Aggregation of human platelets in an annular vortex distal to a tubular expansion. *Microvasc. Res.* 17:217–237, 1979. doi:[10.1016/S0026-2862\(79\)80001-1](https://doi.org/10.1016/S0026-2862(79)80001-1).
- ¹⁵Katsamouris, A. A., A. C. Waltman, M. A. Delichatsios, and C. A. Athanasoulis. Inferior vena cava filters: *in vitro* comparison of clot trapping and flow dynamics. *Radiology* 166:361–366, 1988.
- ¹⁶Keynton, R. S., M. M. Evancho, R. L. Sims, N. V. Rodway, A. Gobin, and S. E. Rittgers. Intimal hyperplasia and wall shear in arterial bypass graft distal anastomoses: an *in vivo* model study. *J. Biomech. Eng.* 123:464–473, 2001. doi:[10.1115/1.1389461](https://doi.org/10.1115/1.1389461).
- ¹⁷Kim, D., R. R. Edelman, C. J. Margolin, D. H. Porter, C. R. McArdle, B. W. Schlam, L. E. Gianturco, J. B. Siegel, and M. Simon. The Simon nitinol filter: evaluation by MR and ultrasound. *Angiology* 43:541–548, 1992. doi:[10.1177/000331979204300701](https://doi.org/10.1177/000331979204300701).
- ¹⁸Komorowicz, E., K. Kolev, I. Lerant, and R. Machovich. Flow rate-modulated dissolution of fibrin with clot-embedded and circulating proteases. *Circ. Res.* 82:1102–1108, 1998.
- ¹⁹Leask, R. L., K. W. Johnston, and M. Ojha. *In vitro* hemodynamic evaluation of a Simon nitinol vena cava filter: possible explanation of IVC occlusion. *J. Vasc. Interv. Radiol.* 12:613–618, 2001. doi:[10.1016/S1051-0443\(07\)61486-9](https://doi.org/10.1016/S1051-0443(07)61486-9).
- ²⁰Leask, R. L., K. W. Johnston, and M. Ojha. Hemodynamic effects of clot entrapment in the TrapEase inferior vena cava filter. *J. Vasc. Interv. Radiol.* 15:485–490, 2004.
- ²¹Liu, W. C., Y. S. Do, S. W. Choo, D. I. Kim, Y. W. Kim, D. K. Kim, S. W. Shin, K. B. Park, Y. H. Jeon, and I. W. Choo. The mid-term efficacy and safety of a permanent nitinol IVC filter (TrapEase). *Korean J. Radiol.* 6:110–116, 2005.
- ²²Lorch, H., A. Dallmann, M. Zwaan, and H. D. Weiss. Efficacy of permanent and retrievable vena cava filters: experimental studies and evaluation of a new device. *Cardiovasc. Intervent. Radiol.* 25:193–199, 2002. doi:[10.1007/s00270-001-0044-4](https://doi.org/10.1007/s00270-001-0044-4).
- ²³Lyman, D. J., S. F. Stewart, J. Murray-Wijelath, and E. Wijelath. Role of fluid dynamics on the healing of an *in vivo* tissue engineered vascular graft. *J. Biomed. Mater. Res. B. Appl. Biomater.* 77:389–400, 2006. doi:[10.1002/jbm.b.30436](https://doi.org/10.1002/jbm.b.30436).
- ²⁴McCowan, T. C., E. J. Ferris, and D. K. Carver. Inferior vena caval filter thrombi: evaluation with intravascular US. *Radiology* 177:783–788, 1990.
- ²⁵McCowan, T. C., E. J. Ferris, D. K. Carver, and W. M. Molpus. Complications of the nitinol vena caval filter. *J. Vasc. Interv. Radiol.* 3:401–408, 1992.
- ²⁶Millward, S. F., J. I. Marsh, C. Pon, and D. Moher. Thrombus-trapping efficiency of the LGM (Vena Tech) and titanium Greenfield filters *in vivo*. *J. Vasc. Interv. Radiol.* 3:103–106, 1992.
- ²⁷Miyazaki, K., T. Nishibe, H. Manase, H. Ohkashiwa, T. Takahashi, S. Watanabe, H. Katoh, and Y. Morita. Gianturco stents for the venous system: a detailed pathological study. *Surg. Today* 28:396–400, 1998. doi:[10.1007/s005950050148](https://doi.org/10.1007/s005950050148).
- ²⁸Mobin-Uddin, K., R. McLean, H. Bolooki, and J. R. Jude. Caval interruption for prevention of pulmonary embolism. Long-term results of a new method. *Arch. Surg.* 99:711–715, 1969.
- ²⁹Mobin-Uddin, K., J. K. Trinkle, and L. R. Bryant. Present status of the inferior vena cava umbrella filter. *Surgery* 70:914–919, 1971.
- ³⁰Nutting, C., and D. Coldwell. Use of a TrapEase device as a temporary caval filter. *J. Vasc. Interv. Radiol.* 12:991–993, 2001.
- ³¹PREPIC Study Group. Eight-year follow-up of patients with permanent vena cava filters in the prevention of pulmonary embolism: the PREPIC (Prevention du Risque d'Embolie Pulmonaire par Interruption Cave) randomized study. *Circulation* 112:416–422, 2005. doi:[10.1161/CIRCULATIONAHA.104.512834](https://doi.org/10.1161/CIRCULATIONAHA.104.512834).
- ³²Robinson, R. A., and I. K. Ilev. Design and optimization of a flexible high-peak-power laser-fiber coupled illumination system used in digital particle imaging velocimetry. *Rev. Sci. Instr.* 75:4856–4862, 2004. doi:[10.1063/1.1809263](https://doi.org/10.1063/1.1809263).
- ³³Rousseau, H., P. Perreault, P. Otal, L. Stockx, J. Golzarian, V. Oliva, P. Reynaud, F. Raat, F. Szatmari, G. Santoro, G. Emanuelli, M. Nonent, and Y. Hoogveen. The 6-F nitinol TrapEase inferior vena cava filter: results of a prospective multicenter trial. *J. Vasc. Interv. Radiol.* 12:299–304, 2001. doi:[10.1016/S1051-0443\(07\)61907-1](https://doi.org/10.1016/S1051-0443(07)61907-1).
- ³⁴Sakharov, D. V., and D. C. Rijken. The effect of flow on lysis of plasma clots in a plasma environment. *Thromb. Haemost.* 83:469–474, 2000.
- ³⁵Silverstein, M. D., J. A. Heit, D. N. Mohr, T. M. Petterson, W. M. O'Fallon, and L. J. Melton, 3rd. Trends in the incidence of deep vein thrombosis and pulmonary embolism: a 25-year population-based study. *Arch. Intern. Med.* 158:585–593, 1998.
- ³⁶Simon, M. Vena cava filters: prevalent misconceptions. *J. Vasc. Interv. Radiol.* 10:1021–1024, 1999. doi:[10.1016/S1051-0443\(99\)70186-7](https://doi.org/10.1016/S1051-0443(99)70186-7).
- ³⁷Simon, M., D. J. Rabkin, S. Kleshinski, D. Kim, and B. J. Ransil. Comparative evaluation of clinically available inferior vena cava filters with an *in vitro* physiologic simulation of the vena cava. *Radiology* 189:769–774, 1993.
- ³⁸Stewart, S. F., and D. J. Lyman. Effects of an artery/vascular graft compliance mismatch on protein transport: a numerical study. *Ann. Biomed. Eng.* 32:991–1006, 2004. doi:[10.1023/B:ABME.0000032462.56207.65](https://doi.org/10.1023/B:ABME.0000032462.56207.65).
- ³⁹Swaminathan, T. N., H. H. Hu, and A. A. Patel. Numerical analysis of the hemodynamics and embolus capture of a Greenfield vena cava filter. *J. Biomech. Eng.* 128:360–370, 2006. doi:[10.1115/1.2187034](https://doi.org/10.1115/1.2187034).
- ⁴⁰Wang, H. Q., L. X. Huang, M. J. Qu, Z. Q. Yan, B. Liu, B. R. Shen, and Z. L. Jiang. Shear stress protects against endothelial regulation of vascular smooth muscle cell migration in a coculture system. *Endothelium* 13:171–180, 2006. doi:[10.1080/10623320600760282](https://doi.org/10.1080/10623320600760282).